Improving the stellarator through advances in plasma theory

C. C. Hegna[1], D. T. Anderson[1], A. Bader[1], T. Bechtel[1], A. Bhattacharjee[2], M. Cole[2], M. Drevlak[3], J. Duff[1], B. J. Faber[1], S. R. Hudson[2], M. Kotschenreuther[4], T. Kruger[1], M. Landreman[5], I. J. McKinney[1], E. Paul[2,9], M. J. Pueschel[6], J. S. Schmitt[6], P. W. Terry[1], A. S. Ware[7], M. Zarnstroff[2], C. Zhu[2]

[1]University of Wisconsin-Madison, Madison, WI, USA [2]Princeton Plasma Physics Laboratory, Princeton, NJ, USA [3]IPP-Greifswald, Greifswald, Germany, [4]University of Texas, Austin, TX, USA [5]University of Maryland, College Park, NJ, USA, [6]Eindhoeven University of Technology, Eindhoven, The Netherlands, [7]Auburn University, Auburn, AL, USA [8]University of Montana, Missoula, MT, USA [9]Princeton University, Princeton, NJ, USA
email: cchegna@wisc.edu

Abstract

Improvements to the stellarator concept can be realized through advancements in theoretical and computational plasma physics. In particular, recent advances are reported in the topical areas of: 1) energetic ion confinement, 2) affecting turbulent transport using 3D shaping, 3) novel optimization and design methods, 4) reducing coil complexity and 5) MHD equilibrium tools. Advances in physics understanding can be used to improve stellarator optimization efforts. These advances enable the development of new stellarator configurations with excellent confinement properties.

1.   INTRODUCTION

The stellarator is unique among magnetic confinement concepts in that the plasma performance is largely determined by externally applied magnetic fields. The flexibility in magnetic configuration design brings both unique challenges and considerable opportunities to improve the stellarator concept. In particular, advancements in plasma theory led to the identification of various optimization approaches including quasi-symmetry, quasi-omnigeneity, etc. that enables the stellarator to overcome the problem of poor neoclassical transport properties at low collisionality. In this work, we highlight recent advances in stellarator theory, computation and modeling motivated by the desire to improve the stellarator concept toward the realization of fusion energy.

Recent success in the stellarator program is driven by the era of the optimized stellarator whereby a particular approach to improving neoclassical transport is the defining characteristic of the magnetic configuration. The successful design, construction and operation of the HSX and W7X configurations affirms the utility of the advanced theoretical concepts in developing magnetic configurations for stellarator. Moreover, theoretical guidance also aided in identifying high performance configurations on LHD and W7AS. However, the basic designs for these configurations were developed a number of decades ago. Significant advances in both theoretical understanding, computational tooks and design techniques have been made in the ensuing years. These advances can be used to address stellarator gaps in various areas and ultimately used to inform advanced stellarator design.

In the next generation of stellarator design, the promising features of neoclassically optimized high-β concepts can be united with new opportunities for advancement that seek to [1]:
- Improve high-energy particle confinement
- Reduce turbulent transport
- Avoid impurity accumulation
- Simplify coil design
- Develop robust divertor systems compatible with good confinement

All of these features are profoundly informed by advancements in plasma theory and computation. In the following, we review recent progress a number of important topical areas. These advances encompass a range of issues including the foundational problem of defining the nature of MHD equilibria in 3D geometry to using 3D shaping to improve energetic particle confinement and reducing turbulent transport consistent with favorable neoclassical transport. Moreover, there have been developments of new algorithmic tools in designing and optimizing promising configurations and simplifying coils. Details in these topical areas are provided in the following sections.

2. ENERGETIC PARTICLE CONFINEMENT

Energetic particle confinement is a key issue for the scalability of stellarators to fusion power plants. Prompt losses of fusion born alpha particles can damage wall components and degrade plasma facing materials. Due to the three-dimensional geometry, trapped particles in unoptimized stellarators often have a radial component to the bounce averaged drift. The various optimization schemes identified to reduce neoclassical transport are never in practice realized exactly. As such, there will inevitably be some level of deviation from the idealized configuration that can lead to prompt energetic particle losses. Indeed, prior energetic particle calculations results from the NCSX design showed that good confinement of thermal particles does not necessarily imply good confinement of energetic particles [2,3].

Previous results indicate that high values of quasisymmetry, an optimization that confines both thermal and energetic particles, can improve alpha particle confinement [4]. Also, the inward shifted LHD configuration which aligns the minima of the magnetic field on a surface has been known to greatly improve confinement [5]. Highly quasi-symmetric quasihelically (QH) symmetric configurations [6] also have been seen to possess this property, as will be shown below.

In order to design stellarator configurations with a high degree of energetic particle confinement, it is prudent to develop easily calculable metrics that effectively quantity losses. Towards this end, a new energetic particle metric, Γ_c, was developed [7] as a measure of how well the contours of the adiabatic invariant align with the magnetic surfaces. The quantity Γ_c is given by

$$\Gamma_c = \frac{\pi}{\sqrt{8}} \lim_{L_s \to \infty} \left(\int_0^{L_s} \frac{ds}{B} \right)^{-1} \left[\int_1^{B_{max}/B_{min}} db' \sum_{well_j} \gamma_c^2 \frac{v\tau_{b,j}}{4B_{min}b'^2} \right]. \tag{1}$$

The crucial quantity to minimized in the optimization scheme is the quantity γ_c given by

$$\gamma_c = \frac{2}{\pi} \arctan\left(\frac{v_r}{v_\theta}\right) \quad , \tag{2}$$

where v_r is the bounced averaged radial drift and v_θ is the bounced averaged poloidal drift. The summation of Eq. (1) is taken over all the magnetic wells for a suitably long field line. The calculation considers wells encountered by all possible trapped particle pitch angles, with b' denoting a normalized value of the magnetic field and $\tau_{b,j}$ denoting the bounce time for a particle in well j. The maximum and minimum values of the magnetic field line are given by B_{max} and B_{min}, respectively.

Using the Γ_c metric in optimization schemes, in conjunction with quasi-helical symmetry, one can consistently produce configurations which eliminate collisionless losses within the half radius for an ARIES-CS scale reactor [8]. While appealing to quasi-symmetry generally improves energetic confinement, the utility of the Γ_c metric in the optimization focuses on improving energetic particle orbits near the trapped-passing boundary. Using advanced optimization algorithms, it is possible to generate equilibria with good energetic particle confinement along with other desirable properties such as the presence of a magnetic well, and a boundary suitable for generation with modular coils [9]. Advances on coil generation algorithms such as FOCUS and REGCOIL have allowed for the demonstration that coils can be designed that reproduce such equilibria with enough fidelity that additional losses from coil-ripple effects are not introduced.

Recently work has been extended to include collisional losses for reactor relevant configurations. Presented separately at this conference [10] is work that seeks to further the connection between configurations with good confinement properties and the neoclassical metrics. Some results for different configurations scaled to have the same volume and magnetic field strength are shown in Figure 1. Alpha particles are sourced in radius given reactor relevant density and temperature profiles and followed with collisions enabled. On the left-hand plot, alpha particle energy loss fraction is given as a function of time. Here we see that the best performing configurations, Wistell-B, Wistell-A and Ku5 are quasi-helically (QH) symmetric configurations. The performance of the quasi-omnigenous configuration, W7-X and the LHD inward shifted configurations are on par with the Wistell-A configuration. The three quasi-axisymmetric (QA) configurations, NCSX, ARIES-CS, and the Henneberg et al [4] configuration perform poorer in comparison, with the best QA performance obtained with the Henneberg et al configuration. The inward shifted LHD configuration performs remarkably better on both energetic particle confinement and the Γ_c metric, compared to the outward shifted configuration.
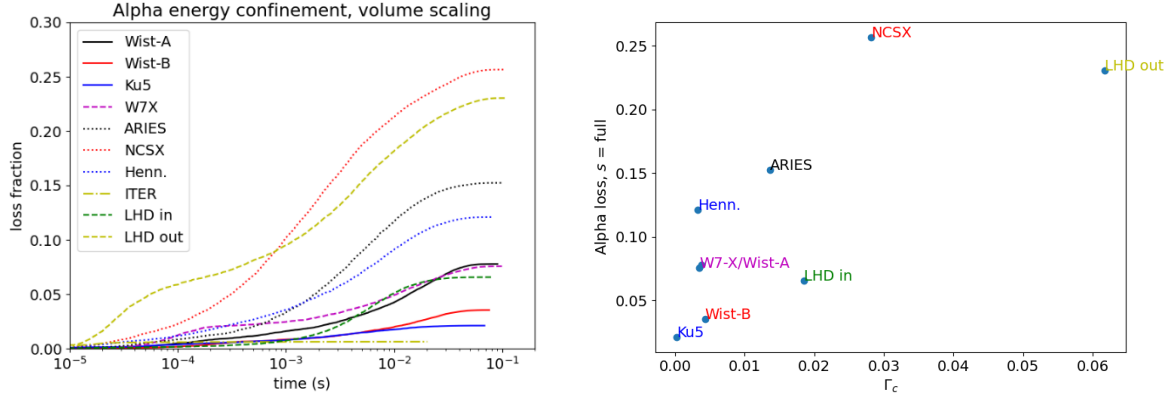
Fig. 1. Left: Energy losses from alpha particle confinement as a function of time for 10 different configurations. Solid lines represent QH configurations, Dotted lines represent QA configurations and dashed lines represent non-quasisymmetric configurations. ITER is included as a reference. Right: total alpha particle energy loss plotted against the neoclassical Γ_c metric for all stellarator configurations.

The right plot in Figure 1 shows the performance of each configuration with respect to the minimum value of the Γ_c metric between $s = 0.2$ and 0.7. In general configurations with better performance in Γ_c perform better in energetic particle confinement. This is especially accurate when considering configurations of the same type (i.e. comparisons between the QH and QA configurations). An expanded discussion on this topic can be found in Ref. [10].

The recipe of minimizing Γ_c together with small deviations from quasi-symmetry has proven to be a robust optimization scheme for producing stellarator configurations with improved energetic particle confinement. Current work includes synthesizing good energetic particle confinement with other physics goals, some of which are described in the following sections. Some work has already been done in combining energetic particle confinement with buildable coils resulting in the Wistell-A configuration [9] whose energetic ion properties are reported here.

3. EFFECT OF 3D SHAPING ON TURBULENT TRANSPORT

The success of 3D magnetic equilibrium optimization in reducing neoclassical transport losses has been demonstrated experimentally in the HSX, LHD and W7-X configurations. As a result, transport in present-day optimized stellarators is dominated by ion-scale microturbulence, driven by Ion Temperature Gradient ITG) modes and Trapped Electron Modes (TEM) in the electrostatic limit, and projections for significant transport from Kinetic Ballooning Modes (KBM) turbulence in stellarator plasmas with finite plasma β. Significant advancements in gyrokinetic and fluid simulations as well as improved analytic theory and modeling capabilities are uncovering new insights on how three-dimensional shaping impacts microturbulence and turbulent transport. This work includes both linear and nonlinear microinstability studies with linear work focusing on the impact of various geometric quantities (curvature, local magnetic shear, trapped particle physics, etc.) on linear growth rates while nonlinear studies concentrate on turbulent saturation physics.

A useful paradigm for identifying the role of 3D shaping on turbulent transport properties is provided by a reduced fluid description. Ion-scale drift wave fluctuations typically have ballooning-like nature quantified by $k_{||}/k_\perp \ll 1$ where $k_{\perp(||)}$ is the perpendicular (parallel) fluctuation wavenumber such that fluctuations are locally perpendicular to the magnetic field at lowest order: $\boldsymbol{k}_\perp \cdot \boldsymbol{B} = 0$. The magnetic field can be written as $\boldsymbol{B} = \nabla\psi \times \nabla\alpha$, where ψ is the toroidal flux function and $\alpha = \theta - \iota\zeta$ labels field lines with θ and ζ straight field line poloidal and toroidal angle coordinates with rotational transform ι. The local perpendicular wavenumber can be written as $\boldsymbol{k}_\perp = k_\alpha(\nabla\alpha_0 + \iota'(\zeta - \zeta_k)\nabla\psi)$, where $\iota' = d\iota/d\psi$ is the global magnetic shear, $\nabla\alpha_0 = \nabla\theta - \iota\nabla\zeta$ and $\zeta_k = k_\psi/\iota'k_\alpha$. Typically, fluid-like instabilities such as ITG satisfy a second ordinary ordinary differential equation for the electrostatic potential ϕ along the magnetic field line for complex eigenvalue ω. A characteristic ITG equation has the following form:

$$(1 + \tfrac{\omega_*}{\omega})(\hat{\boldsymbol{b}} \cdot \nabla)^2 \phi + \omega \omega_d \left(1 + \tfrac{\omega_*}{\omega}\right)\phi + \omega^2 \left(1 + b\left(1 + \tfrac{\omega_*}{\omega}\right)\right)\phi = 0, \tag{3}$$

where $\omega_d = \boldsymbol{k}_\perp \cdot \boldsymbol{v}_d$ is the magnetic drift frequency, $\omega_* = \boldsymbol{k}_\perp \cdot \boldsymbol{v}_*$ is the diamagnetic frequency and $b = k_\perp^2 \rho_s^2$. Both the localization and destabilization is determined by the competition between ω_d, which is destabilizing for negative values, and b, which provides stabilization with increasing positive values. From $k_\perp^2 = k_\alpha^2[\nabla\alpha_0 \cdot \nabla\alpha_0 + 2\iota'(\zeta - \zeta_k)\nabla\psi \cdot \nabla\alpha_0 + \iota'^2(\zeta - \zeta_k)^2 \nabla\psi \cdot \nabla\psi]$, leading contributions to large values of $k_\perp^2$ typically come from either $\nabla\alpha_0 \cdot \nabla\alpha_0$ or from $\iota'^2(\zeta - \zeta_k)^2 \nabla\psi \cdot \nabla\psi$. In many neoclassical transport optimized stellarator designs, the rotational transform profile is constrained within a small range to avoid low order rational surfaces, resulting in small values of ι' (averaged magnetic shear) across the plasma volume. The stabilizing term in $k_\perp^2$ is then dominated by the contribution from $\nabla\alpha_0 \cdot \nabla\alpha_0$ which typically has large "spikes" followed by regions of small value, as demonstrated in Figure (2) for the HSX stellarator. Crucially, each of these $k_\perp^2$ "wells" can localize drift waves, allowing for many unstable solutions to Eq. (3) for a single $k_\perp$, where each mode has a "toroidal"-like nature where the drive is dominated by ω_d. Eq. (3) also simultaneously admits "slab"-like solutions insensitive to local variations in ω_d that extend across multiple $k_\perp^2$ wells. Note that in a typical axisymmetric configuration with moderate magnetic shaping and conventional values of average magnetic shear, the leading contribution to $k_\perp^2$ tends to come from the ι'^2 term with other contributions subdominant and typically only a few toroidal-like unstable eigenmodes exists for a given $k_\perp$.

Figure 2: Dependence of $\nabla\alpha_0 \cdot \nabla\alpha_0$ along a field line in the HSX stellarator.

The effects of low averaged magnetic shear are readily observed in gyrokinetic simulations of ion-scale drift wave instabilities and turbulence in stellarators. Gyrokinetic eigenvalue calculations for the HSX reveal a collection of unstable eigenmodes at each k_α for both ITG and TEM drift waves [11,12], At low k_α, a particularly important branch of eigenmodes have extended slab-lke structure. Rather than play a passive role, these modes are critical to resolving the nonlinear energy dynamics of drift-wave-driven-turbulence. This is observed in density-gradient-driven TEM simulations of HSX, where numerically converged simulations are achieved only when the subdominant and stable slab-like modes are properly resolved by extending the simulation domain multiple poloidal transits along the magnetic field line. Projecting the nonlinear distribution function onto the linear eigenmodes spectrum provides a mechanism for estimating the importance of an eigenmode in the turbulent state. Figure (2) shows the result of such a projection for TEM turbulence in HSX geometry. Notably, Figure (3) shows that the turbulence is dominated by a class of unstable and stable slab-like ITG eigenmodes rather the most unstable toroidal-like modes. The prevalence of these subdominant/slab-like eigenmodes is related to the nonlinear turbulent saturation physics. The strength of the nonlinear saturation transfer plays a central role in predicting the overall turbulent transport rates. Detailed comparison of ITG turbulence in the HSX and the NCSX configurations show HSX has larger normalized dominant linear growth rates for toroidal-like ITG modes at low k_α. However, the level of normalized turbulent transport in HSX is smaller by roughly a factor of 3 compared to NCSX [13]. Analysis of the eigen-spectrum shows only a few toroidal-like modes are destabilized for NCSX, which has magnetic shear values approximately 10 times that of HSX.
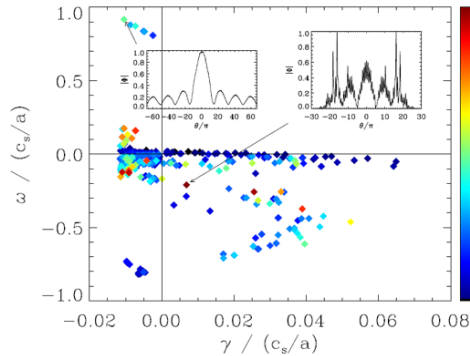
Figure 3: Projection of nonlinear gyrokinetic distribution function onto TEM eigenmodes
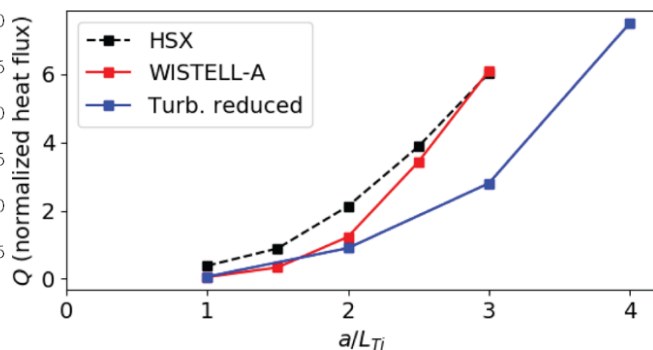
Figure 4: ITG heat fluxes as a function of normalized ion temperature gradient for the HSX and the turbulence reduced configurations.

Leveraging these insights and simulation advances has allowed for the first time the accurate simulation of KBM-driven turbulence in stellarators. Linear gyrokinetic simulations where the linear mode structure is properly resolved by extending the parallel simulation domain show a critical β value for KBM excitation occurs well below the ideal ballooning MHD threshold at long wavelengths. Nevertheless, nonlinear simulations on extended parallel domains not only converge, but show nonlinear stabilization for a range of β larger than the linear critical β with turbulent transport rates that are substantially smaller than electrostatic ITG counterpart [14]. Analysis of the energy dynamics show the dominant energy transfer occurs at small k_α where the extended slab-like modes efficiently couple to both zonal and non-zonal modes. These advances in flux tube simulations are augmented by recent extensions of gyrokinetic codes to full flux annulus and full volume stellarator domains. The XGC-S gyrokinetic code, a stellarator extension of the full volume particle-in-cell XGC code, provides the capability for modeling turbulence in the edge region of stellarators [15]. The first XGC-S results provide some of the first fully global simulations of turbulence in stellarator geometries and is being extended to adapt the electromagnetic XGC pullback operator for stellarator simulations. The Eulerian GENE code has also been extended to incorporate global stellarator geometry [16] and used to examine the role of fully global stellarator geometry on ITG turbulence in standard W7-X configurations [17].

A large body of recent work has also been devoted to understanding the turbulence mechanisms of the quasi-isodynamic W7-X stellarator. A key feature of the quasi-isodynamic design is the parallel adiabatic invariant $J = \int m v_\parallel dl$ is a maximum on the magnetic axis such that $\partial J / \partial \psi < 0$, and is tied to intrinsic TEM stability. Analysis of the power transfer between particle species and turbulent fluctuations yields a necessary condition for TEM instability is the species diamagnetic drift and bounce-averaged magnetic must be positive: $\omega_{*p}\overline{\omega_{dp}} = -\frac{k_\alpha^2 T_p}{e_p^2}\frac{d\ln n_p}{d\psi}\left(\frac{\partial J}{\partial \psi} - \frac{k_\psi}{k_\alpha}\frac{\partial J}{\partial \alpha}\right)$ for species p [18]. For perfectly quasi-isodynamic stellarators, $\partial J / \partial \psi < 0$ and $\partial J / \partial \alpha = 0$ and combined with typical peaked density profiles such that $d\ln n_p /d\psi < 0$ leads to TEM stability. This remarkable property of quasi-isodynamic configurations has been observed in linear instability calculations for W7-X, which is only approximately quasi-isodynamic. A "stability valley" is observed over a range of both density and ion temperature gradients where TEM and ITG growth rates are suppressed [19], where ITG instability suppression is due to non-zero density gradients. This stability valley effect has also been observed in nonlinear flux surface simulations of enhanced performance W7-X discharges [20], where the density gradient driven by pellet fueling substantially suppresses heat fluxes due to ITG turbulence, while the TEM growth rates are largely suppressed due to the maximum-J effect. Proof-of-principle optimizations for TEM turbulence have been performed in a quasi-helically symmetric configuration using this metric and successfully reduced TEM heat fluxes by a factor of two [21].

An important consequence of this research is the observation that traditional quasilinear models [12] are insufficient for predicting turbulent transport in quasisymmetric stellarators. This observation is motivating the construction of new reduced models and theories to investigate how 3D geometry affect drift wave instabilities and turbulent saturation physics. The basic paradigm of this work is the prevalence of three-wave interactions mediating the transfer of energy from unstable to damped eigenmodes as the dominant saturation mechanisms. Theories based on these ideas have been used to explain finite-β stabilization of turbulence [22-24] and the Dimits shift [25] in tokamak application. A new fluid model capturing the coupling between unstable and stable ITG modes with full 3D geometry information has been constructed [26]. Coupling between unstable and stable modes is largely determined by a three-wave interaction time: $\tau_{pst}(k, k') = \left[i\left(\omega_t(k'') + \omega_s(k') - \omega_p^*(k)\right)\right]^{-1}$ where $\omega_p(k)$ is the primary ITG instability at wavenumber k, $\omega_s(k')$ is a damped (stable) mode at wavnumber k', and $\omega_t(k'')$ is a third mode at wavenumber $k'' = k - k'$. Large values of τ_{pst} indicate favorable coupling between the unstable and stable modes, potentially allowing for increased energy transfer from the unstable to the stable modes. Application of the model to different classes of quasisymmetric equilibria reveal a strong dependence of the dominant saturation channel on 3D geometry. For quasiaxisymmetric configurations, linear instabilities couple to damped modes most effectively through zonal flows with negligible frequency, however for quasihelically symmetric configurations the dominant coupling mechanism is through finite frequency, non-zonal modes yielding an order-of-magnitude larger τ_{pst} values than for the zonal-flow-mediated coupling. This strong non-zonal coupling in the quasihelically symmetric configuration is enabled both by the slab-like modes that have relatively weak $k_\perp$ dependence and by the fact that toroidal-like modes can be localized by the local shear to the same location along the magnetic field line, resulting in similar frequencies.

Although these results are obtained for ITG, complementary studies have been performed for TEM instabilities. Kotschenreuther and co-workers have recently shown from non-equilibrium thermodynamic principles that drift wave

eigenfunctions can "decouple" from the trapped particles when the eigenfunction becomes sufficiently narrow along a magnetic field line. This can occur both in the strongly shaped edge region of tokamaks and in stellarators where the local shear serves to localize eigenfunctions in a narrow $k_\perp^2$ well. This provides a physical route by which turbulent transport may be reduced for both ITG and TEM-driven turbulence in low global magnetic shear quasisymmetric stellarators. By keeping the global magnetic shear small, the large variations in the local shear encourage resonant interactions between unstable and stable toroidal-like ITG modes localized to the same $k_\perp^2$ well, slab-like ITG and TEM modes can provide efficient coupling mechanisms to damped modes, and enhanced local shear confinement can induce decoupling of the locally trapped electron population. These effects are observed in the turbulence reduced configuration presented in [9], where reduced turbulent is observed across of range of gradient scale lengths for ITG turbulence, as seen in Figure (4).

4.   STELLARATOR COILS

Stellarator coils are one of the most expensive components of stellarators. The difficulties in designing and fabricating complicated non-planar coils partly led to the cancellation of the NCSX project and the delay of the W7-X experiment. This critical challenge of stellarator coils comes from two parts, complex geometry and tight tolerance. In the past years, the stellarator community has made significant improvements in theory and computation to reduce the coil complexity and increase the tolerance [27]. These efforts can be divided into the following three categories.

New coil design methods have been developed. One of the main approaches to designing stellarator coils is to solve a least squared minimization problem. In this approach, the surface current potential on a pre-scribed winding surface is computed using the Green's function [28]. Fundamentally, this problem is ill-posed. The original regularization in the NESCOIL code is to simply truncate the Fourier spectrum. Landreman [29] developed a new code, REGCOIL, and employed a Tikhonov regularization over the squared current density. REGCOIL can simultaneously improve the free-boundary reconstruction of the target plasma shape while substantially increasing the minimum distances between coils. Paul et al. [30] extended the REGCOIL code by allowing the winding surface to be varied. In this approach, the adjoint method described in the following section is used to construct the required derivative information resulting in a substantial decrease in computation cost.

A different approach was advanced by Zhu et al. [31] in which coils are described using fully 3D representation without the necessity of providing a winding surface. Based on this idea, a new coil design code FOCUS has been developed [32]. By getting rid of the winding surface, FOCUS-designed coils can be moved freely in the space and consequently explore more possible coil designs. FOCUS uses analytically calculated derivatives to accelerate the speed and improve robustness. Recently, a new curvature constraint was implemented in FOCUS [33].

There are also other new coil design methods. For example, new codes have been developed that considering the finite-build effect of the coil [34,35]. A new trend is to combine plasma optimization and coil design [36]. Indeed, numeral tools have been developed that can simultaneously optimize coil shapes using the near-axis quasi-symmetry approach described in Section 5 [37] or updating the magnetic field data for a free-boundary VMEC calculation [38]

With all the new methods, we are now able to design coils for the next-generation stellarators. For example, in the optimized energetic particle calculations described in Section 2, FOCUS is used to design coils that adequately reproduce the excellent alpha particle properties of these configurations.

Coil tolerance can be better handled. The plasma response is sensitive to magnetic field perturbations. Even small error fields might have a large impact on plasma confinement. Accuracy requirements were the largest driver for the cost growth of NCSX [39]. To address the tight tolerance of stellarator coils, several methods have been proposed. As to be discussed in Section 5, the concept of shape gradients is a powerful tool to address this problem. As the shape gradient gives the local differential contribution to some scalar figure of merit (shape functional) caused by normal displacements, it can be used to compute the local sensitivity and tolerances for coils.

Coil design is essentially an optimization problem. It is expected that the ideal coils will be close to the local minimum of the figure of merit. In this circumstance, the gradient is negligible, and a quadratic approximation is applicable. Hence, the Hessian matrix provides the sensitivity information [40]. Instead of performing computationally expensive perturbation analysis to scan possible deviations, eigenvalues of the Hessian matrix indicate the impact of coil perturbations on plasma properties. The first principal eigenvector, which is associated with the largest eigenvalue,

will have the most significant effect on error fields. The Hessian matrix method is demonstrated on CFQS to identify the coil perturbations that will enlarge magnetic islands or deteriorate the quasi-symmetry of the magnetic field [41].
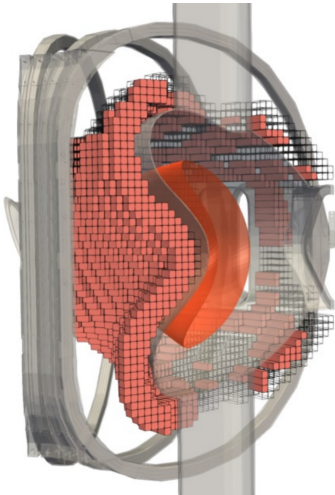
Figure 5: One-sixth of the half-Tesla NCSX experiment with permanent magnetics and TF coils.

Permanent magnets will simplify stellarator coils. To date, only electromagnetic coils have been used to generate 3D fields for stellarators. Permanent magnets provide an alternative way to produce the desired magnetic field for optimized stellarators. The idea of using permanent magnets to simplify stellarator coils has been evolved rapidly. The initial proposal was to use a curl-free, "one-sided" magnetization volume generating the required poloidal field, as permanent magnets cannot create toroidal magnetic flux [42]. It is also possible to replace the surface current potential with a layer of perpendicular magnetic dipoles [43]. An efficient linear-least-squares method has been demonstrated in which permanent magnets can have arbitrary direction [44] and also topology optimization has been developed [45]. The new code, FAMUS, can design engineering-feasible permanent magnets for general stellarators satisfying the constraints of the maximum material magnetization and explicitly forbidden regions. Together with the geometric code, MAGPIE, [46], FAMUS is able to design simple permanent magnets with planar TF coils for a half-Tesla NCSX configuration. The design has good accuracy in generating the desired equilibrium and offers considerably large plasma access on the outboard side. The results led to a recently-awarded proposal to construct one-sixth of the permanent magnets for the experiment, as illustrated in figure 5.

5.   NOVEL OPTIMIZATION METHODS

Substantial progress has been made in optimization and design methods for stellarators. One example is a new method to generate and parameterize quasi-symmetric and omnigenous plasma configurations using analytic expansions about the magnetic axis [47-50]. The reduction of the equations for MHD equilibrium and quasisymmetry afforded by this approach makes it possible to compute and analyze equilibria several orders of magnitude faster than in traditional stellarator optimization, on times comparable to a millisecond rather than tens of seconds. This speed-up enables wide surveys over parameter space. The simplification of the equations also makes it possible to obtain insights into the space of solutions, such as a precise characterization of the set of configurations that are quasisymmetric to first order in distance from the axis. Many physical properties can be computed directly and analytically from a near-axis solution, including Mercier stability and all the geometric quantities entering the gyrokinetic equation, with no need for a full finite-aspect-ratio 3D MHD numerical solution [51]. An example quasi-helically symmetric configuration constructed from the near-axis expansion technique is provided in Fig. 6.
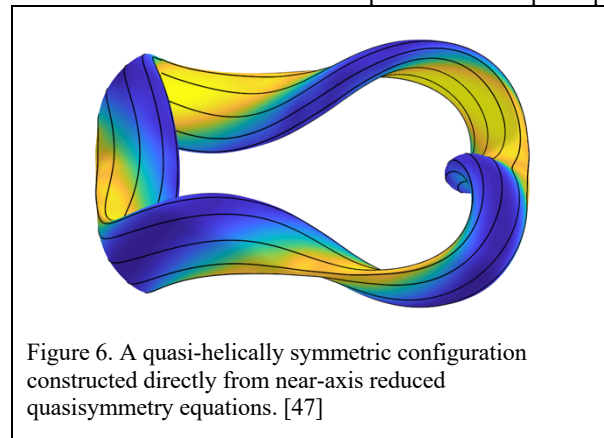
Figure 6. A quasi-helically symmetric configuration constructed directly from near-axis reduced quasisymmetry equations. [47]
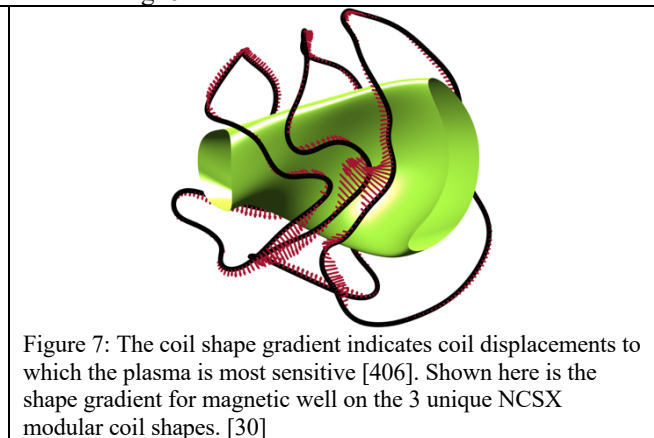
Figure 7: The coil shape gradient indicates coil displacements to which the plasma is most sensitive [406]. Shown here is the shape gradient for magnetic well on the 3 unique NCSX modular coil shapes. [30]

Another area of progress is the development of adjoint methods for computing shape gradients. These techniques, widely used outside of plasma physics, allow derivatives to be computed extremely efficiently. These derivatives are valuable both for optimization and sensitivity analysis. For a numerical calculation that depends on N parameters, to evaluate the derivative of the calculation with respect to all parameters by finite differences, the calculation must be

repeated N times, with a step taken in each direction in parameter space. However, adjoint methods allow the same N derivatives to be evaluated with only a single linear calculation of cost no greater than the original "forward problem". This reduction in computational cost from $O(N^1)$ to $O(N^0)$ is a tremendous gain, especially when optimizing shapes, where N can be arbitrarily high. Adjoint techniques have great promise for stellarator fusion plasma physics since the shapes of flux surfaces and electromagnetic coils must be optimized, and the sensitivity of the coil shapes is critical. Shape gradients on coils can provide tolerance information, as they represent displacements of the coils to which the plasma physics properties are sensitive [52], as shown in figure 7. Adjoint methods have recently been derived for many quantities of interest for stellarator design, including collisional transport, coil complexity, and the width of magnetic islands. [30,53-55]. Derivative-based optimization using these adjoint methods has been demonstrated in the past year for obtaining desirable MHD properties [54] and quasisymmetry [37], and to maximize the volume of good surfaces [55]. Two examples are shown in figures 8 and 9.
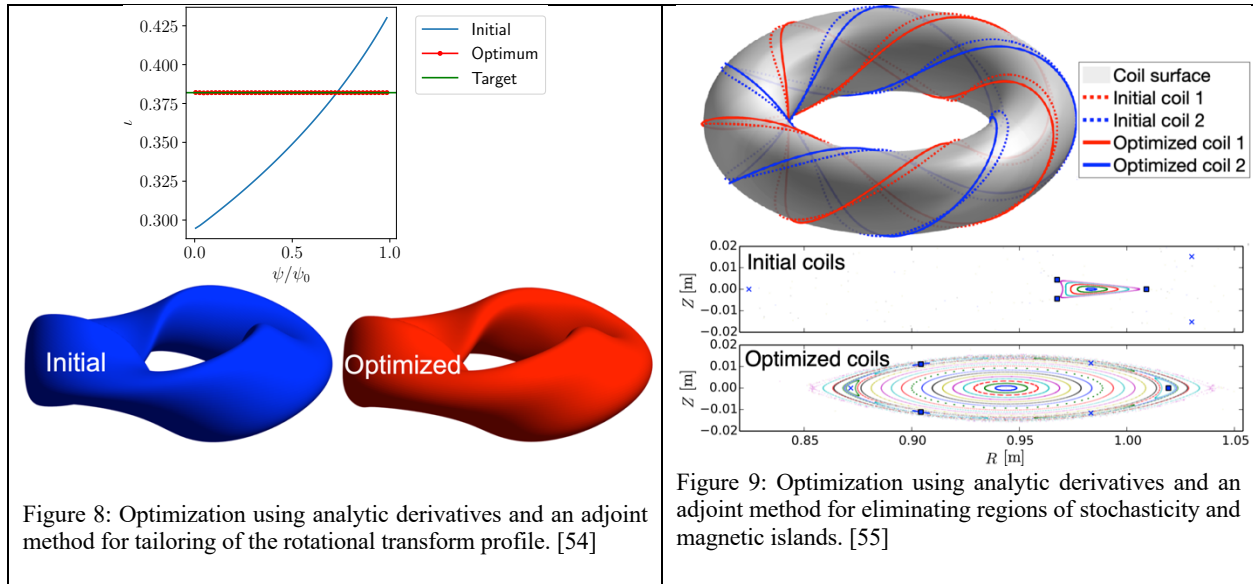
Figure 8: Optimization using analytic derivatives and an adjoint method for tailoring of the rotational transform profile. [54]

Figure 9: Optimization using analytic derivatives and an adjoint method for eliminating regions of stochasticity and magnetic islands. [55]

Together, the near-axis expansion and adjoint methods have enabled the first combined plasma-and-coil optimization for quasisymmetry that uses analytic derivatives [37]. The independent variables consist of both coil shapes and parameters for a near-axis plasma configuration. Consistency between the two is obtained by a penalty in the objective function. The simplification of the quasisymmetry condition by the near-axis expansion allows derivatives of the objective to be obtained by an adjoint method, making optimization very efficient. An example of a configuration obtained by this method is shown in figure 10.

Another novel optimization technique that benefits stellarator design is "stochastic optimization" [56,57]. In this approach, used already in finance and other subjects, the optimization problem is formulated to account for uncertainty, yielding optima that are more robust. This can be done by taking the objective function to be an expectation value over a distribution of possible realizations, with the expectation value computed by an average over samples. In the context of stellarators, there is uncertainty in the coil shapes due to finite tolerances in manufacturing and assembly. Using stochastic optimization, groups at IPP and NYU have demonstrated coil designs that better preserve desired properties of the confined plasma in the presence of coil shape errors [56,57]. One comparison of stochastic and deterministic optimization is shown in figure 11. Stochastic optimization also helps to smooth over narrow local minima in the objective function, yielding improved optima even in the absence of coil errors.
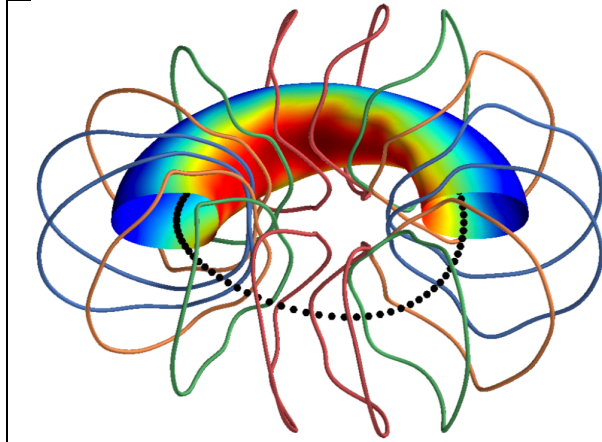
Figure 10. A quasi-axisymmetric configuration and coils obtained using single-stage derivative-based optimization. [37]
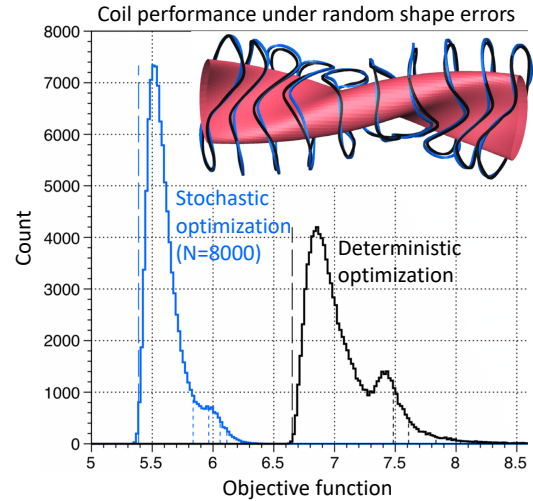
Figure 11. Using stochastic optimization, robust coils can be found that yield a small value of the objective function even in the presence of random deviations in the coil shapes. [56]

6. MHD EQUILIBRIUM TOOLS

Stellarators are instrinsically three-dimensional (3D). As has long been known, mathematical pathologies generally arise in 3D MHD equilibria at rational flux surfaces. So-called δ-function current-densities arise if the constraints of ideal MHD are imposed. Though not problematic from a theoretical perspective, they do create discontinuities in the tangential magnetic field. The allowance of discontinuous magnetic fields at a dense set of rational surfaces is problematic from a numerical perspective. Another singularity is the pressure-driven "$1/x$" current-density. To avoid nonphysical parallel plasma currents in arbitrary geometry, the pressure gradient must vanish in a non-zero neighborhood around each rational surface. In resistive MHD, rational flux surfaces will break apart into islands and, where these islands overlap, regions of irregular field lines that ergodically cover volumes will arise. From the MHD equilibrium condition, $\boldsymbol{B} \cdot \nabla p = 0$, the pressure is constant along magnetic field lines. For nonintegrable magnetic fields, this *is* a problem. If the region of interest is a fractal mix of good flux surfaces, which can support radial pressure gradients, and magnetic islands and irregular field lines, which cannot, the pressure profile becomes a fractal devil's staircase.

To overcome these mathematical pathologies and motivated by a theorem presented by Bruno & Laurence [58] that, provided certain conditions are met, guarantees the existence of a special class of sharp-boundary equilibria now known as *stepped pressure* equilibria, the stepped-pressure equilibrium code (SPEC) was developed [59]. The underlying theoretical model is called multi-region relaxed MHD (MRxMHD). The plasma domain is partitioned into N_V nested subregions. The multi-region energy functional is $W = \sum_i \int \left(\frac{p}{(\gamma - 1)} + B^2/2 \right) dv$, is minimized subject to the constraint that the helicity in each volume, $H_i = \int \boldsymbol{A}.\boldsymbol{B} \, dv$, is conserved. Rather than seeking differentiable solutions, *weak* solutions are sought that allow for discontinuities in p and $\boldsymbol{B}$ at the interfaces. The extremizing equations are that in the i-th subregion the magnetic field obeys $\nabla \times \boldsymbol{B}_i = \mu_i \boldsymbol{B}_i$, where $\mu_i = const.$ is formally a Lagrange multiplier used to enforce the helicity constraint, and across the ideal interfaces the total pressure is continuous, $[p + B^2/2] = 0$. Hence, the equilibrium can be viewed as a nested set of Taylor states. As the constraints of ideal MHD are *not* globally imposed, reconnection and magnetic islands are allowed. The ideal current singularities that otherwise arise at rational surfaces are eliminated. The subregions are separated by *ideal interfaces*, at which the constraints of ideal MHD are imposed. These can support pressure. The global pressure profile is approximated by a piecewise-stepped profile with a discrete number of pressure jumps at the interfaces. The interfaces are required to have irrational rotational-transform so as to avoid the classical problem of singular currents.

SPEC builds upon the strong foundation laid by the VMEC code [60], which is widely used in the stellarator community. Both codes seek minima of the energy functional; however, VMEC restricts the search to equilibria with continuous integrable magnetic fields and applies the ideal constraint globally. In contrast, SPEC allows for discontinuous nonintegrable fields and applies the ideal constraint only at a finite set of interfaces. SPEC eliminates the mathematical pathologies at rational surfaces in integrable ideal equilibria. And, crucially for stellarator optimization calculations, SPEC provides a self-consistent measure of island width. In the limit of an infinite number of interfaces ($N_V = \infty$), MRxMHD recovers ideal MHD [61]. The topological constraints of ideal MHD are imposed globally, and smooth pressure profiles are accommodated. We have verified that in this case SPEC accurately computes the aforementioned δ-function and pressure-driven $1/x$ current-densities of ideal MHD [62] and the Rosenbluth singular solution [63] at resonant surfaces [64].
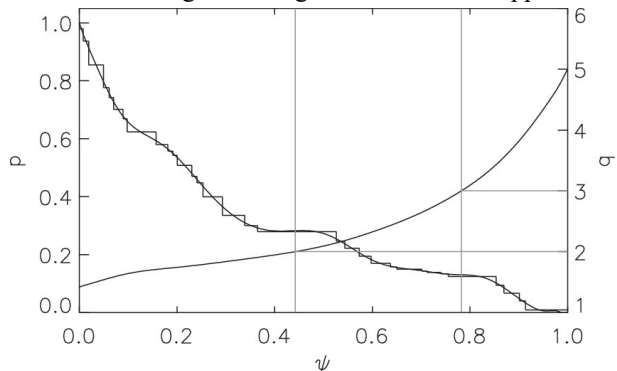
Figure 12: SPEC reconstruction of DIII-D equilibrium profiles in the presence of applied magnetic fields.

When N_V is finite, the equilibrium is generally a mix of islands at the rational surfaces and pressure jumps at a selection of irrational surfaces. The size of the islands is determined by the shape of the plasma boundary. A typical stepped-pressure equilibrium is shown in Figs. 12 and 13. The pressure (p) and safety-factor (q) profiles were obtained from a reconstruction of DIIID with applied resonant magnetic perturbations [65].
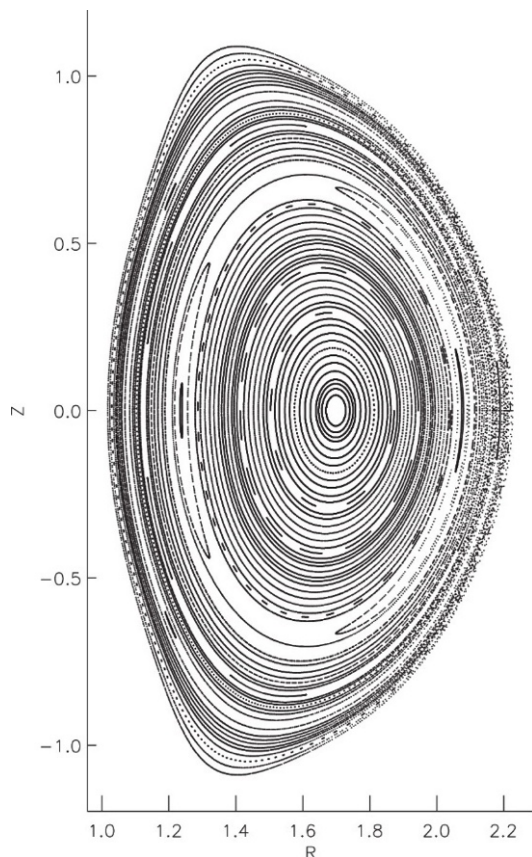
Figure 13: The magnetic topology associated with the SPEC reconstruction of Figure shows an m = 2 magnetic island.

For *equilibrium* calculations, the given profiles impose topological constraints on the magnetic field. To see this, we note than an equilibrium code *by definition* computes the magnetic field consistent with force balance, $\nabla p = j \times B$, with the given profiles and the geometry of the plasma boundary (for free boundary calculations, the external magnetic field must be provided). To compute the equilibrium magnetic field for a *given* pressure profile, where there are pressure gradients, the equilibrium magnetic field *must* have flux surfaces for it to be consistent with $B \cdot \nabla p = 0$. It is only where the pressure profile is flat that the equilibrium magnetic field may have islands and/or chaos. A Poincaré plot of the magnetic field that is consistent with the profiles shown in Figure 11 is shown in Figure 12 and a magnetic island can be seen at the $q = 2$ surface, where the pressure is constant.

SPEC has been used to compute the width of saturated nonlinear tearing modes in 3D equilibra, and this calculation has been verified against analytic predictions [66]. For the SPEC measures of island widths to be used in stellarator optimization calculations, this is an important verification exercise. As described above, in the ideal $N_v \rightarrow \infty$ limit, these islands are "shielded-out" by imposed topological constraints. In this case, the magnitude of the singular current densities may be used as a proxy for magnetic island width.

In addition to computing MRxMHD equilibrium states, SPEC can compute their linear stability. In the $N_V = \infty$ limit, this agrees with ideal stability [67]. The theoretical model has been extended to include flow [68]. Rather than just using the theoretical model of MRxMHD to construct equilibria, a fully dynamical version of MRxMD based on Lagrangian variational principles has been derived [69]. SPEC has been used to study the equilibrium β-limit in classical stellarators [70]. A free-boundary capability has recently been developed [71].

There are ongoing efforts to incorporate SPEC into various stellarator optimization algorithms. VMEC is still the faster and easier code to use. Many existing equilibrium post-processing codes (which may assess neoclassical transport, for example) used in stellarator optimization still require a VMEC equilibrium as input, and VMEC is still the basis of most stellarator optimization efforts. Recently, the SPEC development team is shifting its attention from code verification to code optimization.

Equilibrium codes such as VMEC and SPEC are essential for both configuration optimization and equilibrium reconstruction. However, equilibrium codes have their limits. A number of physical effects outside of the MHD equilibrium model are known to impact magnetic island formation and hence, magnetic topology in 3-D configurations. Driven by this need, there are ongoing efforts to broaden the applicability of the extended MHD tools NIMROD, M3D-C1 and JOREK for stellarator applications [72,73]. In these tools the effects of plasma resistivty, neoclassical effects, plasma flow effects, etc, can be accommodated. Moreover, these tools can also be employed to assess the nonlinear consequences of stellarators breaching MHD instability boundaries.

7. CONFIGURATION DESIGN

The various advances in physics understanding can be used to generate metrics for use in the stellarator optimization codes STELLOPT and ROSE. These advances are being employed to produce new stellarator configurations with excellent confinement properties. In recent years, example configurations based on the quasi-axiymmetric [4] and quasi-helically symmetric [9] optimization principle with a mixture of the improved confinement properties described here. These designs benefit from advances in the coil design. Figure 14 shows a representation of the coils for the Wistell-A configuration described in [4] using the FOCUS code. The right panel of Fig. 14 shows a Poincare plot of the magnetic surfaces obtained from these coils in vacuum.
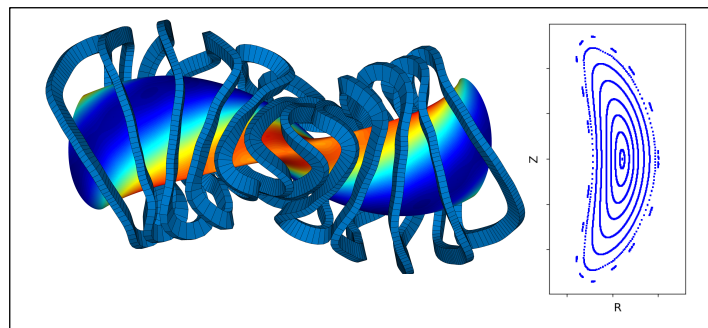
Figure 14: Representation of the coils for the Wistell-A configuration. A Poincare plot for the magnetic surfaces produced by these coils in vacuum is provided in the right panel.

REFERENCES

[1] D. A. Gates, et al *J. Fusion Energy* **37**, 51 (2018).
[2] H. E. Mynick, A. H. Boozer, and L. P. Ku, *Phys. Plasmas* **13**, 064505 (2006).
[3] L. P. Ku and P. R. Garabedian, *Fusion Sci, Technol* **50**, 207 (2006).
[4] S. A. Henneberg, M. Drevlak and P. Helander, *Plasma Phys. Control. Fusion* **62**, 014023 (2020).
[5] H. E. Mynick, *Phys. Plasmas* **13**, 058102 (2006).
[6] L. P. Ku and A. H. Boozer, *Nuclear Fusion* **51**, 013004 (2011).
[7] V. V. Nemov, S. V. Kasilov and W. Kernbichler, *Phys. Plasmas* **21**, 062501 (2014).
[8] A. Bader et al, *J. Plasmas Physics* **85**. 90580508 (2019).
[9] A. Bader et al, *J. Plasmas Physics* **86**, 90580506 (2020).
[10] A. Bader et al, "Improving Energetic Ion Confinement in Stellarator Reactors," IAEA FEC (2021).
[11] B. J. Faber et al, *J. Plasmas Physics* **84**, 905840503 (2018).
[12] M. J. Pueschel et al, *Phys. Rev. Lett.* **116**, 085001 (2016).
[13] I. J. McKinney et al, *J Plasmas Physics* **85**, 905850503 (2019).
[14] I. J. McKinney et al, submitted to *J. Plasmas Physics* (2021).
[15] M. Cole et al, *Phys. Plasmas* **27**, 044501 (2020).
[16] M. Maurer et al, *J. Comp. Phys.* **420**, 109694 (2020)
[17] A. Bañón Navarro et al, *Plasma Phys. Controlled Fusion* **62**, 105005 (2020)
[18] P. Helander et al, *Phys. Plasmas* **20**, 122505 (2013)

[19] J. A. Alcusón et al, *Plasma Phys. Controlled Fusion*, **62**, 035005 (2020)
[20] P. Xanthopoulos et al, *Phys. Rev. Lett.* **125**, 075001 (2020)
[21] J. H. E. Proll et al, *Plasma Phys. Controlled Fusion*, **58**, 014006 (2016)
[22] P. W. Terry et al, *Phys. Plasmas* **25**, 012308 (2018).
[23] G. G. Whelan et al, *Phys. Rev. Lett.* **120**, 175002 (2018)
[24] G. G. Whelan et al, *Phys. Plasmas* **26**, 082302 (2019).
[25] P. W. Terry et al, *Phys. Rev. Lett.* **126**, 025004 (2021).
[26] C. C. Hegna et al, *Phys. Plasmas* **25**, 022511 (2018).
[27] C. Zhu et al, "Towards simpler coils for optimized stellarators," IAEA, FEC (2021).
[28] P. Merkel, *Nucl. Fusion* **27**, 867 (1987)
[29] M. Landreman, *Nucl. Fusion* **57**, 046003 (2017).
[30] E. Paul et al, *Nucl. Fusion* **58**, 076015 (2018).
[31] C. X. Zhu, S. R. Hudson, Y. T. Song and Y. W, Wan, *Nucl. Fusion* **58**, 016008 (2018)
[32] C. X. Zhu, S. R. Hudson, Y. T. Song and Y. W. Wan, *Plasmas Phys. Controlled Fusion* **60**, 065008 (2018).
[33] T. G. Kruger et al *Journal of Plasmas Physics* **87**, 175870201 (2021).
[34] L. Singh et al, *J. Plasma Physics* **86**, 905860404 (2020).
[35] N. McGreivy, S. R. Hudson and C. Zhu, *Nucl. Fusion* **61**, 026020 (2021).
[36] S. R. Hudson, C. Zhu, D. Pfefferle and L Gunderson *Physics. Letters A.* **382**, 2732 (2018).
[37] A. Giuliani et al, arXiv:2010.02033 (2020).
[38] T. Brown, "Advancement of the PPPL straight leg Quasi-axisymmetric stellarator design," IAEA FEC (2021).
[39] R. L. Strykowsky et al, *23rd IEEE/NPSS Symposium on Fusion Engineering*, 345 (2009).
[40] C. X. Zhu et al, *Plasma Phys. Controlled. Fusion* **60**, 054016 (2018).
[41] C. X. Zhu et al, *Nuclear Fusion* **59**, 126007 (2019).
[42] P. Helander, M. Drevlak, M. Zarnstorff and S. C. Cowley, *Phys. Rev. Letter* **124**, 095001(2020).
[43] C. X. Zhu, M. Zarnstorff, D. A. Gates and A. Brooks, *Nuclear Fusion* **60**, 076016 (2020).
[44] M. Landreman and C. Zhu, *Plasmas Phys. Controlled Fusion* **63**, 035001 (2021).
[45] C. X. Zhu et al, *Nuclear Fusion* **60**, 106002 (2020).
[46] K. C. Hammond et al, *Nuclear Fusion* **60**, 106010 (2020).
[47] M. Landreman and W. Sengupta*, J Plasma Phys* **85**, 815850601 (2019).
[48] G. Plunk, M. Landreman and P. Helander, *J Plasma Phys* **85**, 905850602 (2019).
[49] R. Jorge, W. Sengupta, and M. Landreman, *Nucl. Fusion* **60**, 076021 (2020).
[50] E. Rodriguez and A. Bhattacharjee, *Phys Plasmas* **28**, 012508 (2021).
[51] R. Jorge and M. Landreman, *Plasma Phys. Controlled Fusion* **63**, 014001 (2020).
[52] M. Landreman and E. Paul, *Nucl. Fusion* **58**, 076023 (2018).
[53] T. Antonsen, E. Paul, and M. Landreman, *J Plasma Phys* **85**, 905850207 (2019).
[54] E. Paul, M. Landreman, and T. Antonsen, arXiv:2012.10028 (2020).
[55] A. Geraldini, M. Landreman, and E. Paul, arXiv:2102.04497 (2021).
[56] J. F. Lobsien et al, *Nucl. Fusion* **58** 106013 (2018)
[57] J. F. Lobsien et al, *J Plasma Phys* **86**, 815860202 (2020)
[58] O. P. Bruno and P. Lawrence, *Communications on Pure and Applied Mathematics* **49**, 717 (1996).
[59] S. R. Hudson et al, *Phys. Plasmas* **19**, 112502 (2012)
[60] S. P. Hirshman and W. I. Van Rij, *Computer Physics Communications* **43**, 143 (1986).
[61] G.R. Dennis et al, *Phys. Plasmas* **20**, 032509 (2013).
[62] J. Loizu et al, *Phys. Plasmas* **22**, 090704 (2015).
[63] M. N. Rosenbluth, R. Y. Dagazian and P. H. Rutherford, *Phys. Fluids* **16**, 1894 (1973).
[64] Huang et al, manuscript in preparation (2021).
[65] S. A. Lazerson et al, "3D Equilibrium effects on DIII-D," 39th EPS Conference, p. 4077 (2012).
[66] J. Loizu et al, *Phys. Plasmas* **27**, 070701 (2020).
[67] A. Kumar et al, *Plasma Phys. Controlled Fusion* **63**, 045006 (2021).
[68] Z. S. Qu et al, *Plasmas Phys. Controlled Fusion* **62**, 054002 (2020).
[69] R. L. Dewar et al, *J. Plasma Phys.* **81**, 515810604 (2015).
[70] J. Loizu et al, *J. Plasmas Physics* **83**, 715830601 (2017).
[71] S. R. Hudson et al, *Plasmas Phys. Controlled Fusion* **62**, 084002 (2020).
[72] M. G. Schlutt et al, *Nuclear Fusion* **52**, 103023 (2012); M. G. Schlutt et al, *Phys. Plasmas* **20**, 056104 (2013).
[73] T. A. Bechtel et al, to be submitted to *Phys. Plasmas* (2021).